RSC Advances

PAPER

View Article Online
View Journal | View Issue

Cite this: *RSC Adv.*, 2023, **13**, 20958

Dielectric chiral metasurfaces for enhanced circular dichroism spectroscopy at near infrared regime

Asif Ali,†[a] Hafiz Saad Khaliq, †[ad] Aqsa Asad,†[a] Jehan Akbar,[b] Muhammad Zubair, *[c] Muhammad Qasim Mehmood *[a] and Yehia Massoud*[c]

Numerous applications of chiro-optical effects can be found in nanophotonics, including imaging and spin-selective absorption, particularly in sensing for separating and detecting chiral enantiomers. Flat single-layer metasurfaces composed of chiral or achiral sub-wavelength structures offer unique properties to manipulate the light due to their extraordinary light–matter interaction. However, at optical wavelengths, the generation of strong chirality is found to be challenging *via* conventional chiral metasurface approaches. This work intends to design and optimize a dielectric chiral meta-nano-surface based on a diatomic design strategy to comprehend giant chiro-optical effects in the near-infrared (NIR) regime for potential application in circular dichroism (CD) spectroscopy. Instead of using a single chiral structure that limits the CD value at optical wavelengths, the proposed metasurface used a diatomic (two meta-atoms with distinct geometric parameters) chiral structure as a building block to significantly enhance the chiro-optical effect. Combining both meta-atoms in a single periodicity of the building block introduces constructive and destructive interferences to attain the maximum circular dichroism value exceeding 75%. Moreover, using multipolar resonance theory, the physics behind the generation of giant chiro-optical effects have also been investigated. The proposed dielectric chiral meta-platform based on the extra degree of freedom can find application in compact integrated optical setups for CD spectroscopy, enantiomer separation and detection, spin-dependent color filters, and beam splitters.

Received 10th April 2023
Accepted 20th June 2023

DOI: 10.1039/d3ra02331a

rsc.li/rsc-advances

1 Introduction

Over the last two decades, artificially designed materials, metamaterials, and metasurfaces have gained considerable interest due to their extraordinary properties to manipulate electromagnetic (EM) waves for various applications.[1–8] Meanwhile, chiral metamaterials have been investigated for several potential applications in our daily life, such as sensing, imaging, ultrathin polarizers, *etc.*[6,7,9–12] However, fabrication ease and extra freedom in chiral metasurfaces (the planar version of chiral metamaterials) made them the more convenient solution for application in chiral optics.[13–26] In chiral light–matter interaction, metasurfaces introduce chiro-optical effects, mainly categorized as circular-birefringence, circular dichroism (CD), or circular conversion dichroism (CCD). Circular birefringence, also termed optical activity (OA) is defined as the change in polarization of light passing through the optically active material, whereas CD is the differential absorption of both spins of circularly polarized (CP) light.

In recent years, many chiral metasurfaces were presented in the literature based on plasmonic structures to enhance light–matter interaction.[27–30] However, the ohmic losses, enhancement of just electric dipoles, and suppression of higher-order multipolar resonances in such structures at optical wavelengths limit their potential applicability. The technology trend shifted towards high refractive index dielectric nanostructures to mitigate these limitations to enhance the light–matter interaction in near and far-field at the nanoscale.[7,31–36] The concurrent activation of electric and magnetic dipolar resonances in dielectric nanostructures enables them to be used to design Huygens metasurfaces. Furthermore, several groups have presented planar and multilayer dielectric chiral metasurfaces for strong chiro-optical responses based on chiral, achiral, and cascaded geometries.[30,31,35–38] Initially, conventional chiral geometries are demonstrated to achieve strong CD at the selected wavelengths in the infrared regime.[30,35] Then, multilayer chiral metasurfaces were presented for broadband chiro-optical responses based on achiral nanostructures.[36] Meanwhile, planar metasurfaces are also demonstrated based on disks-type structures and cascaded

[a]*MicroNano Lab, Deaprtment of Electrical Engineering, Information Technology University (ITU) of the Punjab, Ferozepur Road, Lahore 54600, Pakistan. E-mail: qasim.mehmood@itu.edu.pk*

[b]*Glasgow College, University of Electronic Science and Technology of China. Chengdu, China*

[c]*Innovative Technologies Laboratories (ITL), King Abdullah University of Science and Technology (KASUT), Saudi Arabia. E-mail: yehia.massoud@kaust.edu.sa; muhammad.zubair3@kaust.edu.sa*

[d]*School of Electronic and Electrical Engineering, Kyungpook National University, Daegu 41566, Republic of Korea*

† Equally contributing authors.

chiral and achiral geometries using nano-rods to achieve significant chiro-optical responses.[31,37,38] A few groups have also presented chiral metasurfaces in the literature based on bound states in the continuum (BICs).[16,39,40] Presumably, for enantiomeric separation and detection, there is still more room to investigate multiple design strategies, specifically the structures optimized for multiband chiro-optical responses at broadband optical wavelengths.

This work presents a compact solution for circular dichroism spectroscopy based on planar dielectric chiral metasurface. A cascaded geometry is designed and investigated based on two hydrogenated amorphous silicon (a-Si:H) L-shaped distinct chiral meta-atoms. Compared to a single meta-atom, a couple of meta-atoms behave as a building block, working in reflective mode and significantly contributing towards polarization-conserved strong chiro-optical effects in the near-infrared (NIR) regime. Moreover, the underlying mechanism behind the generation of strong chiral responses is investigated using multipolar decomposition theory. The individual contribution for each higher-order multipolar resonance is presented based on the excitation of CP light. Furthermore, the oblique incident analysis for the designed meta-platform is also illustrated, which can be a vital feature for the spectroscopic analysis of chiral molecules. Additionally, the proposed dielectric chiral meta-platform incorporates the ability to integrate with on-chip devices to increase its functionality as a compact CD spectroscopic meta-platform.

2 Design, optimization, and results

The schematic illustration of the working principle and design strategy of the proposed diatomic metasurface is depicted in Fig. 1. The proposed diatomic nanostructures are designed by hydrogenated amorphous silicon (a-Si:H) on glass (SiO_2), whereas gold is used as the reflector. The unit cell was optimized using Finite Difference Time Domain (FDTD) method with periodic boundaries in the *x*- and *y*-plane and perfectly matched layer boundaries in the *z*-direction. For simulations to achieve strong chiro-optical effects, the NIR regime was used as the solution wavelengths, and a plane-wave source with circular polarization was used to excite the proposed structure. Initially, instead of a diatomic structure, a single L-type structure was

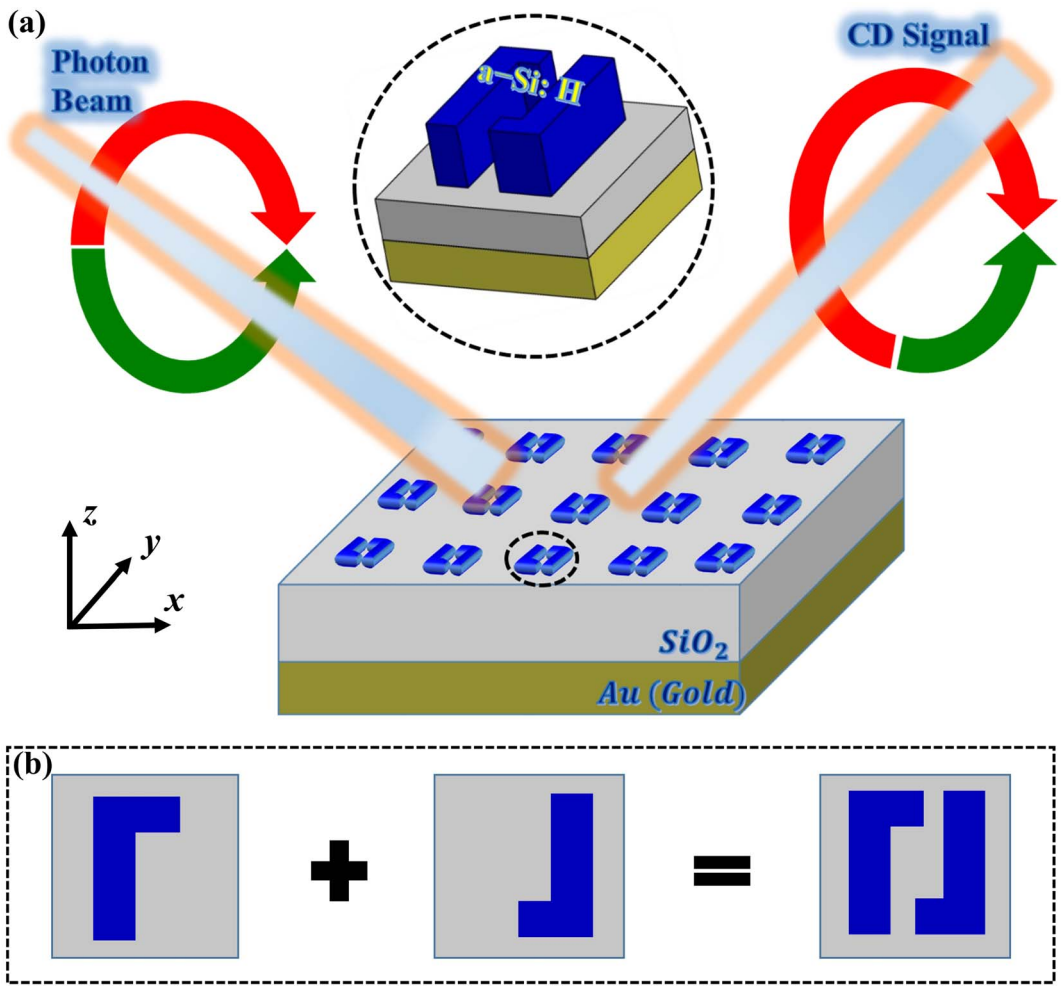

Fig. 1 The artistic view of the working principle and the design strategy of the proposed diatomic flat nano-surface. (a) The reflective nano-surface composed of hydrogenated amorphous silicon-based meta-atoms produces CD signals for enhanced spectroscopy. Inset shows the diatomic chiral structure comprises a pair of symmetry-breaking meta-atoms. (b) The design strategy of the proposed diatomic system.

optimized using a parametric sweep for all the design parameters. After carefully optimizing a single L-type structure and analyzing the chiro-optical responses, a diatomic structure was created using a combination of a pair of single structures. The optimization and the comparative analysis of optical responses for single and diatomic structures are also discussed later in this section. Based on the optimized diatomic configuration, the metasurface provides the giant circular dichroism (CD) at the working wavelengths for enhanced spectroscopy. Meanwhile, due to the symmetry-breaking structure, it conserved the polarization of reflected light. Using Jones calculus, the reflected field can be expressed as in eqn (1) (ref. 10 and 41)

$$\begin{pmatrix} E_r^{\,x} \\ E_r^{\,y} \end{pmatrix} = \begin{bmatrix} r_{xx} & r_{xy} \\ r_{yx} & r_{yy} \end{bmatrix} \begin{pmatrix} E_i^{\,x} \\ E_i^{\,y} \end{pmatrix} = [R] \begin{pmatrix} E_i^{\,x} \\ E_i^{\,y} \end{pmatrix} \quad (1)$$

where R is the reflection matrix, $E_r^{\,x}$ and $E_r^{\,y}$ termed as the reflected electric fields whereas $E_i^{\,x}$ and $E_i^{\,y}$ denote the incident electric fields with polarization in x- and y-direction, respectively. After conversion from linear to CP excitation, the reflection matrix can be written as in eqn (2) (ref. 42)

$$R_{\text{cir}} = \frac{1}{2}\begin{bmatrix} r_{xx} + r_{yy} + i(r_{xy} - r_{yx}) & r_{xx} - r_{yy} - i(r_{xy} + r_{yx}) \\ r_{xx} - r_{yy} + i(r_{xy} + r_{yx}) & r_{xx} + r_{yy} - i(r_{xy} - r_{yx}) \end{bmatrix} = \begin{bmatrix} r_{++} & r_{+-} \\ r_{-+} & r_{--} \end{bmatrix} \quad (2)$$

where the '+' and '−' in subscripts denote the notation for the right and left-handed CP waves, respectively. While for the suggested structure, the following conditions should be considered in eqn (2) as $r_{++} = r_{--} = r_{-+} = 0$ and $r_{+-} = 1$ to obtain the required spin-conserved reflectance. Given these conditions for the proposed reflective symmetry-breaking diatomic structure, the following linear reflection matrix was obtained as expressed in eqn (3):

$$R = e^{j\tau} \times \frac{1}{2}\begin{bmatrix} 1 & j \\ j & -1 \end{bmatrix} \quad (3)$$

where τ denotes the phase shift that occurs in reflected EM waves. Using eqn (3) in (1) and multiplying with the incident CP light expression proves the reflection with polarization conservation for one spin and absorption for the opposite spin.

The perspective and top view of the chiral structure with structural parameters is depicted in Fig. 2(a) and (b), respectively. The optimization of length (L_1) and width (W) parameters for the diatomic meta-atom for optimal values to achieve strong polarization conserved CD response at multiband of NIR regime is shown in Fig. 2. The co-polarized component of reflectance for RCP illumination against length and width at the design wavelength of 896 nm, 970 nm, 996 nm, and 1030 nm is depicted in Fig. 2(c)–(f), respectively. Similarly, the co-polarized part of reflectance for LCP illumination against length and width at the wavelength of 896 nm, 970 nm, 996 nm, and

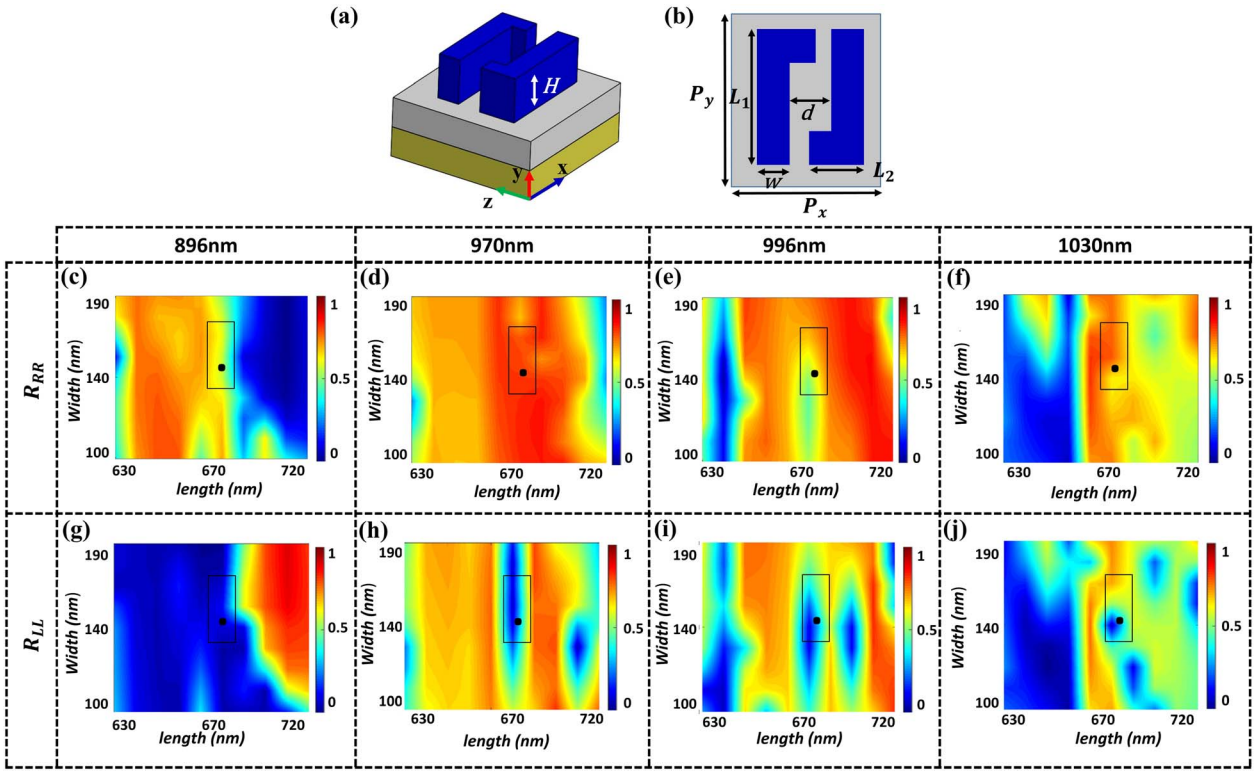

Fig. 2 Parametric optimization of proposed diatomic chiral structure to realize the optimum value of length and width for CP illumination. (a) The perspective and (b) the top view of the chiral structure with design parameters. For the optimum selection of length and width parameters, the co-polarized reflectance is demonstrated at the working wavelengths of (c and g) 896 nm (d and h) 970 nm (e and i) 996 nm (f and j) 1030 nm for RCP and LCP excitation, respectively. The black dots denote the optimum value for maximum circular dichroism at the working wavelengths. R_{RR}: Co-polarized reflectance for RCP incidence, R_{LL}: Co-polarized reflectance for LCP incidence.

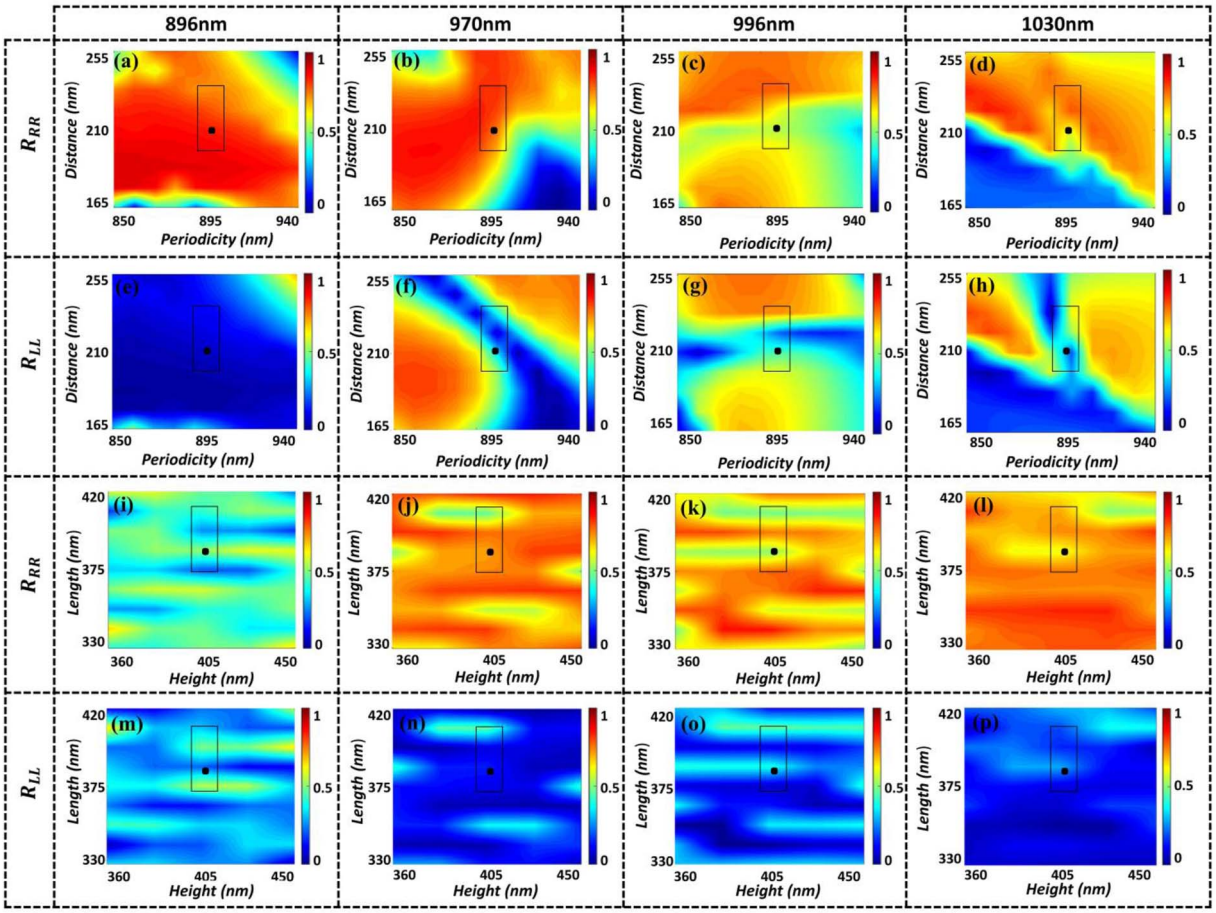

Fig. 3 Parametric optimization of proposed diatomic chiral structure to realize the optimum periodicity, the center distance between both meta-atoms, length (L_2), and height. For the optimum selection of periodicity (P) and the central distance (d) parameter, the co-polarized reflectance is demonstrated at the working wavelengths of (a and e) 896 nm (b and f) 970 nm (c and g) 996 nm (d and h) 1030 nm for RCP and LCP excitation, respectively. Similarly, for the optimum selection of length (L_2) and height (H) parameters, the co-polarized reflectance is demonstrated at the working wavelengths of (i and m) 896 nm (j and n) 970 nm (k and o) 996 nm (l and p) 1030 nm for RCP and LCP excitation, respectively. The black dots denote the optimum value for maximum circular dichroism at the working wavelengths.

1030 nm is depicted in Fig. 2(g)–(j), respectively. The inset black dots in the plots denote the optimal values for the length and width, which can provide maximum CD response at the working wavelengths. Meanwhile, the optimization performed for optimal periodicity (P) ($P_x = P_y = P$), the distance (d) (the gap between both meta-atoms), the arm length (L_2) and height (H) to check the sensitivity of diatomic geometry is illustrated in Fig. 3. The co-polarized part of reflectance for RCP and LCP excitation against periodicity and the central distance at the working wavelengths is shown in Fig. 3(a)–(h), respectively. Likewise, the co-polarized part of reflectance for RCP and LCP excitation against length (L_2) and height (H) at the working wavelengths is depicted in Fig. 3(i)–(p), respectively. The black dots represent the optimal selected values for the mentioned parameters. After careful optimization, the optimal values for the structural parameters of the proposed diatomic structure are given as periodicity (P): 900 nm, height (H): 400 nm, length (L_1): 680 nm, length (L_2): 385 nm, width (W): 150 nm, and distance (d): 310 nm.

For enhanced CD spectroscopy, two enantiomers are designed based on the proposed geometry. A comparative analysis based on the reflectance and the CD response is performed, as illustrated in Fig. 4, when a single L-type meta-atom is simulated instead of a diatomic structure. When just the L1 meta-atom is considered, Fig. 4(a) and (e) depict the reflection parameters and the CD response, respectively. These results show the minimum reflectance for the co-polarized part of reflectance parameters (R_{RR}: RCP reflectance/RCP incident, R_{LL}: LCP reflectance/LCP incident), eventually the CD response is not good at the working wavelengths. Likewise, the L_2 meta-atom (Fig. 4(b) and (f)) demonstrates the small intensity in terms of co-polarized reflectance and the CD response, respectively. In contrast, combining both meta-atoms to make a diatomic structure with optimal central distance can significantly improve co-polarized reflectance and the CD response at the working wavelengths. Fig. 4(c) and (g) demonstrate the reflection parameters and the CD response for enantiomer A of the diatomic geometry. Similarly, Fig. 4(d) and (e) illustrate the reflection parameters and the CD response for enantiomer B, respectively. These results show the maximum co-polarized reflectance for RCP excitation in the case of enantiomer A, whereas the maximum reflectance for LCP illumination in

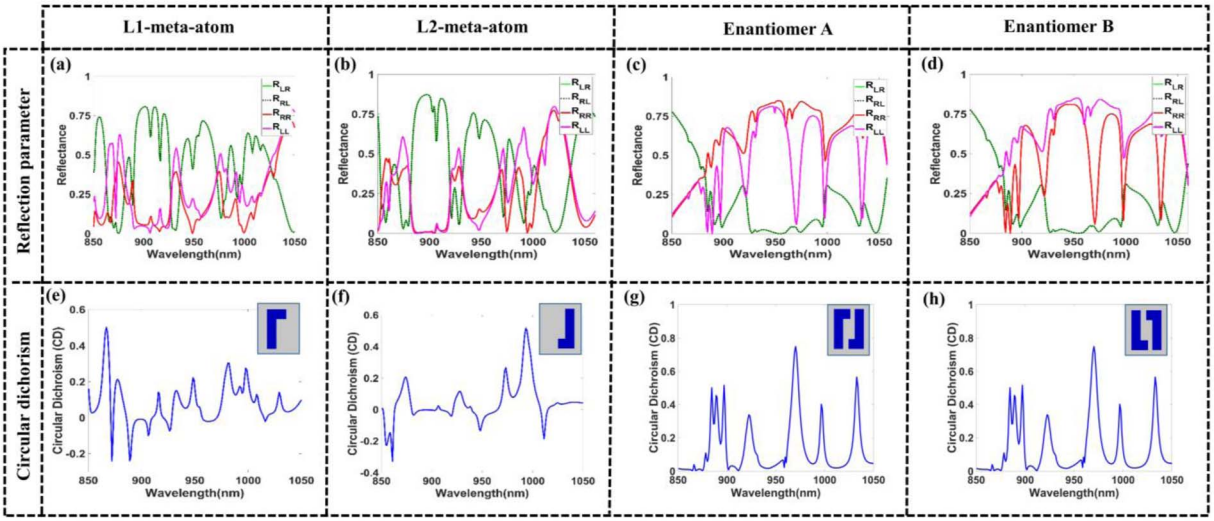

Fig. 4 Demonstration of reflection parameters and circular dichroism of single atoms compared to diatomic unit-atom. The reflection parameters for (a) L_1-meta-atom and (b) L2-meta-atom at the optimal design parameters. The circular dichroism for (e) L_1-meta-atom and (f) L_2-meta-atom. (c) The reflection parameters and (g) the CD for the diatomic chiral structure (enantiomer A) shows the enhancement in chirality compared to a single atom structure. (d) The reflection parameters and (h) the circular dichroism for the enantiomer B of the proposed diatomic chiral system.

enantiomer B. The maximum CD response was achieved for both diatomic structure enantiomers at the working wavelengths for multiband CD spectroscopy in the NIR regime.

Moreover, oblique incident analysis was performed for the diatomic chiral structure to check the dependence of the reflectance parameters for CP illumination. Fig. 5(a) and (b) depicts the reflectance parameters for incident angle in azimuth (*xz*-plane) plane in a range of 0°–80° for CP incident light, respectively. It shows no apparent difference in the reflectance compared to the normal incident light. Meanwhile, the

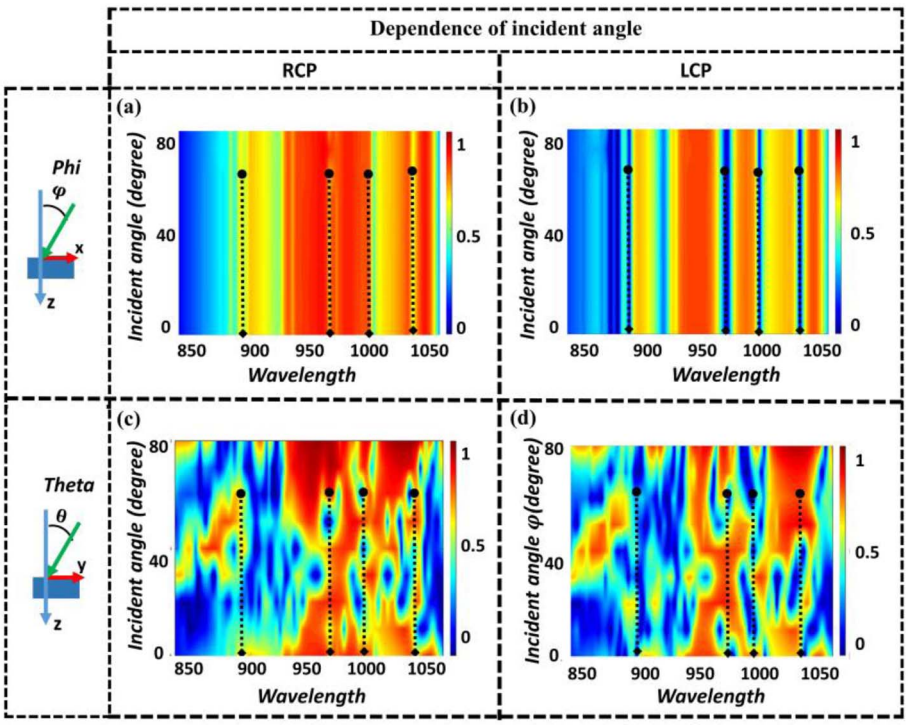

Fig. 5 The chirality dependence on the illumination angle of light. The reflectance for (a) RCP and (b) LCP illumination concerning illumination angle in azimuth-plane in a range of 0–80°. Meanwhile, the reflectance for illumination angle in the elevation plane is demonstrated for (c) RCP and (d) LCP light. The inset dotted lines show the working wavelengths.

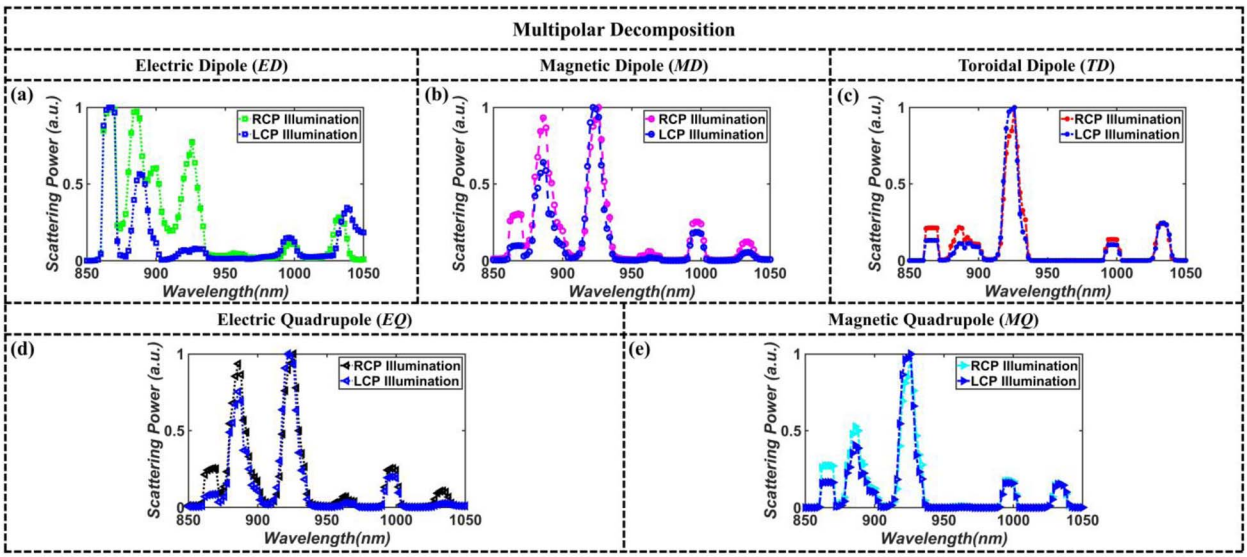

Fig. 6 Spin-dependent multipole decomposition for the diatomic structure. Multipolar decomposition of scattering power for designed chiral diatomic chiral system in terms of (a) electric dipole, (b) magnetic dipole, (c) toroidal dipole, (d) electric quadrupole, (e) magnetic quadrupole for CP illumination. The spin-dependent multipolar resonances demonstrate the significant contribution towards giant circular dichroism in the NIR regime.

reflectance parameters for incident angle in elevation (*yz*-plane) plane in a range of 0°–80° shows the change for RCP (Fig. 5(c)) and LCP (Fig. 5(d)) illumination. However, the proposed chiral metasurface can still detect the enantiomers with some sacrificed CD response at the working wavelengths.

Furthermore, spin-dependent multipolar decomposition is performed for CP incident light to elucidate the generation of giant chirality at multiband in the NIR regime for the designed diatomic dielectric structure.[18,42–46] Fig. 6 depicts the decomposition of normalized scattering power in terms of electric dipole (ED) (Fig. 6(a)), magnetic dipole (MD) (Fig. 6(b)), toroidal dipole (TD) (Fig. 6(c)), electric quadrupole (EQ) (Fig. 6(d)), and magnetic quadrupole (MQ) (Fig. 6(e)) for CP illumination in reflective mode. The multipolar resonances include the combined effect of both meta-atoms in the diatomic building block to contribute toward giant circular dichroism. Each multipolar resonance significantly contributing to induce circular dichroism in the NIR regime, specifically at the working wavelengths. Moreover, it is noticeable from the results that ED, MD, and EQ are more dominant toward giant circular dichroism at all the wavelengths.

The proposed diatomic structure is re-optimized at visible, longer wavelengths in NIR and MIR regimes to check the possibility of working in other wavelength regimes. Fig. 7 depicts the reflectance parameters for the re-optimized or scaled-down/scaled-up structure in the visible regime (Fig. 7(a)), longer NIR regime (Fig. 7(b)), and MIR regime (Fig. 7(c)). The results show the better intensity of multiband chirality in the visible regime at just longer wavelengths exceeding 600 nm due to the absorption loss of chosen material at shorter wavelengths. Meanwhile, chirality illustrated around 1600 nm in longer wavelengths of the NIR regime. The results can be further improved if all the parameters of the proposed structure are optimized simultaneously, which will require high computational power. However, no chirality was obtained in the MIR regime using the scale-up feature for the parameters in the

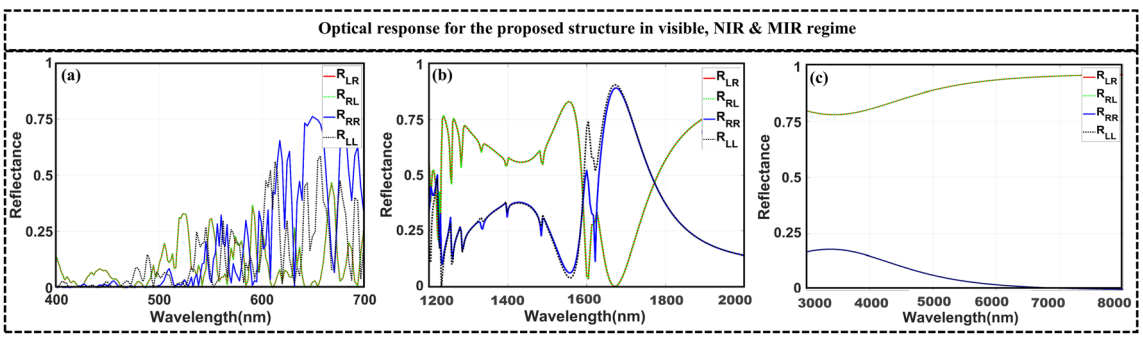

Fig. 7 Reflectance in visible, NIR, and MIR regimes. The reflectance parameters for the proposed structure are in (a) visible, (b) near-infrared (NIR), and (c) mid-infrared (MIR) regimes. It shows the chirality in visible and NIR regimes at multiple wavelengths but no chirality in MIR regimes.

proposed structure, but it can be further optimized to achieve the chiro-optical effects. Consequently, the designed diatomic meta-platform working in a visible, broad NIR regime with significant CD at multiband incorporates the ability for chiral absorption, spin-selective molecular separation and detection, and CD spectroscopic analysis. Moreover, extending the proposed structure in the MIR regime is possible for broadband spectroscopic analysis.

3 Conclusion

In summary, a compact all-dielectric chiral metasurface is proposed based on a diatomic design strategy with extra degree of freedom to realize the giant chiro-optical effects in the near-infrared (NIR) regime. A pair of distinct chiral meta-atoms engineered carefully and merged together to work as the building block. It has been proved by the reflectance parameters that the mutual contribution of both meta-atoms in a diatomic chiral structure leads to giant chiro-optical effects compared to a single meta-atom. Meanwhile, the individual contribution of multipolar resonances towards the generation of giant circular dichroism is also investigated in terms of scattering power using multipolar decomposition theory. Moreover, the proposed structure can be extendable in visible and MIR regime depends on the properties of the used material. The proposed chiral meta-platform with a diatomic design strategy incorporating extra degrees of freedom can have promising applications in integrated nanophotonics for compact CD spectroscopy solutions, enantiomer separation and detection, optical setups for polarimetry,[28,29] data encryption,[27,47] and spin-selective color filters.

Data availability

The datasets used and analyzed during the current study are available from the corresponding authors upon reasonable request.

Conflicts of interest

The authors declare no conflict of interest.

References

1 H.-H. Hsiao, C. Hung Chu, D. Ping Tsai, H. Hsiao, C. H. Chu and D. P. Tsai, *Small Methods*, 2017, **1**, 1600064.
2 W. Jan Krzysztofik and T. Nghia Cao, in *Metamaterials and Metasurfaces*, 2019.
3 S. Noureen, M. Q. Mehmood, M. Ali, B. Rehman, M. Zubair and Y. Massoud, *Nanoscale*, 2022, **14**, 16436–16449.
4 A. Asad, H. S. Khaliq, N. Mahmood and Y. Massoud, Helicity multiplexed wavefront shaping at broadband ultraviolet regime, Holography, Diffractive Optics, and Applications XII, *Proc. SPIE*, 2022, vol. 12318, p. 1231807.
5 A. Asad, J. Kim, H. S. Khaliq, N. Mahmood, J. Akbar, M. T. S. Chani, Y. Kim, D. Jeon, M. Zubair, M. Q. Mehmood, Y. Massoud and J. Rho, *Nanoscale Horiz.*, 2023, **8**, 759–766.
6 J. Kim, J. Seong, W. Kim, G. Y. Lee, S. Kim, H. Kim, S. W. Moon, D. K. Oh, Y. Yang, J. Park, J. Jang, Y. Kim, M. Jeong, C. Park, H. Choi, G. Jeon, K. il Lee, D. H. Yoon, N. Park, B. Lee, H. Lee and J. Rho, *Nat. Mater.*, 2023, **22**(4), 474–481.
7 S. So, J. Mun, J. Park, J. Rho, S. So, J. Mun, J. Rho and J. Park, *Adv. Mater.*, 2023, 2206399.
8 J. Jang, M. Jeong, J. Lee, S. Kim, H. Yun, J. Rho, J. Jang, J. Lee, H. Yun, J. Rho, M. Jeong and S. Kim, *Adv. Mater.*, 2023, **35**, 2203889.
9 A. Lininger, G. Palermo, A. Guglielmelli, G. Nicoletta, M. Goel, M. Hinczewski and G. Strangi, *Adv. Mater.*, 2022, 2107325.
10 H. S. Khaliq, M. R. Akram, K. Riaz, K. Riaz, M. A. Ansari, J. Akbar, J. Zhang, W. Zhu, D. Zhang, X. Wang, M. Zubair, M. Q. Mehmood and M. Q. Mehmood, *Opt. Express*, 2021, **29**(3), 3230–3242.
11 N. A. Kotov, L. M. Liz-Marzán and P. S. Weiss, *ACS Nano*, 2021, **15**, 12457–12460.
12 H. S. Khaliq, I. Kim, J. Kim, D. K. Oh, M. Zubair, K. Riaz, M. Q. Mehmood and J. Rho, *Adv. Opt. Mater.*, 2021, **9**, 2002002.
13 S. S. Bukhari, J. Vardaxoglou and W. Whittow, *Appl. Sci.*, 2019, **9**, 2727.
14 H. S. Khaliq, A. Nauman, J. W. Lee and H. R. Kim, *Adv. Opt. Mater.*, 2023, 2300644.
15 T. Naeem, J. Kim, H. S. Khaliq, J. Seong, M. T. S. Chani, T. Tauqeer, M. Q. Mehmood, Y. Massoud and J. Rho, *Adv. Opt. Mater.*, 2023, **11**, 2202278.
16 A. Overvig, N. Yu and A. Alù, *Phys. Rev. Lett.*, 2021, **126**, 073001.
17 Y. Liang, H. Lin, K. Koshelev, F. Zhang, Y. Yang, J. Wu, Y. Kivshar and B. Jia, *Nano Lett.*, 2021, **21**, 1090–1095.
18 H. S. Khaliq, I. Kim, A. Zahid, J. Kim, T. Lee, T. Badloe, Y. Kim, M. Zubair, M. Zubair, K. Riaz, K. Riaz, M. Q. Mehmood, M. Q. Mehmood, J. Rho, J. Rho, J. Rho and J. Rho, *Photonics Res.*, 2021, **9**(9), 1667–1674.
19 H. S. Khaliq, J. Kim, T. Naeem, K. Riaz, T. Badloe, J. Seong, J. Akbar, M. Zubair, M. Q. Mehmood, Y. Massoud and J. Rho, *Adv. Opt. Mater.*, 2022, 2201175.
20 H. S. Khaliq, I. Kim, K. Riaz, T. Naeem, M. Zubair, J. Rho and M. Q. Mehmood, *J. Phys.: Conf. Ser.*, 2021, **2015**, 012060.
21 Z. Han, F. Wang, J. Sun, X. Wang and Z. Tang, *Adv. Mater.*, 2023, **35**, 2206141.
22 H. S. Khaliq, K. Riaz, M. Zubair and M. Q. Mehmood, in *2021 34th General Assembly and Scientific Symposium of the International Union of Radio Science*, URSI GASS 2021, Institute of Electrical and Electronics Engineers Inc., 2021.
23 T. Naeem, H. S. Khaliq, M. Zubair, T. Tauqeer and M. Q. Mehmood, *RSC Adv.*, 2021, **11**, 13220–13228.
24 C. Chen, S. Gao, W. Song, H. Li, S.-N. Zhu and T. Li, *Nano Lett.*, 2021, **21**(4), 1815–1821.
25 H. S. Khaliq, M. Q. Mehmood and Y. Massoud, *Frontiers in Optics + Laser Science 2022 (FIO, LS)*, 2022, paper JTu5B.7.

26 T. Naeem, H. S. Khaliq, M. Zubair, T. Tauqeer, M. Q. Mehmood and Y. Massoud, *Proceedings of the IEEE Conference on Nanotechnology*, 2022, 2022-July, pp. 190–193.
27 Y. Chen, X. Yang and J. Gao, *Light: Sci. Appl.*, 2019, **8**(1), 1–9.
28 L. Li, J. Wang, L. Kang, W. Liu, L. Yu, B. Zheng, M. L. Brongersma, D. H. Werner, S. Lan, Y. Shi, Y. Xu and X. Wang, *ACS Nano*, 2020, **14**, 16634–16642.
29 Q. Jiang, B. Du, M. Jiang, D. Liu, Z. Liu, B. Li, Z. Liu, F. Lin, X. Zhu and Z. Fang, *Nanoscale*, 2020, **12**, 5906–5913.
30 Z. Shen, S. Fan, W. Yin, S. Li, Y. Xu, L. Zhang, X. Chen, Z. Shen, W. Yin, S. Li, Y. Xu, L. Zhang, X. Chen and S. Fan, *Laser Photonics Rev.*, 2022, **16**, 2200370.
31 F. R. Gómez, J. R. Mejía-Salazar and P. Albella, *ACS Omega*, 2019, **4**, 21041–21047.
32 H. S. Khaliq, T. Naeem, K. Riaz, M. Zubair, M. Q. Mehmood and Y. Massoud, *Proceedings of the IEEE Conference on Nanotechnology*, 2022, 2022-July, pp. 194–197.
33 A. Asad, H. S. Khaliq, A. Zahid, M. Q. Mehmood and Y. Massoud, Uniform chirality enhanced optical responses *via* broadband achiral metasurfaces for bio-sensing applications Nanophotonics, Micro/Nano Optics, and Plasmonics VIII, *Proc. SPIE*, 2023, vol. 12322, p. 123220A.
34 H. S. Khaliq, I. Kim, K. Riaz, T. Naeem, M. Zubair, J. Rho and M. Q. Mehmood, Chiroptical effect induced by achiral structures for full dimensional manipulation of optical waves, High Contrast Metastructures X, *Proc. SPIE*, 2021, vol. 11695, p. 116951M.
35 Y. Gong, S. A. Maier, M. Hong, W. Wang, X. Liu, H. Guo and W. Lu, *Opt. Express*, 2018, **26**(5), 6067–6078.
36 K. Tanaka, D. Arslan, S. Fasold, M. Steinert, J. Sautter, M. Falkner, T. Pertsch, M. Decker and I. Staude, *ACS Nano*, 2020, **14**, 15926–15935.
37 J. Hu, M. Lawrence and J. A. Dionne, *ACS Photonics*, 2020, **7**, 36–42.
38 K. Yao and Y. Zheng, *J. Phys. Chem. C*, 2019, **123**, 11814–11822.
39 K.-H. Kim, J.-R. Kim, K.-H. Kim and J.-R. Kim, *Adv. Opt. Mater.*, 2021, **9**, 2101162.
40 J. Wu, X. Xu, X. Su, S. Zhao, C. Wu, Y. Sun, Y. Li, F. Wu, Z. Guo, H. Jiang and H. Chen, *Phys. Rev. Appl.*, 2021, **16**, 064018.
41 A. C. Overvig, S. Shrestha, S. C. Malek, M. Lu, A. Stein, C. Zheng and N. Yu, *Light: Sci. Appl.*, 2019, **8**(1), 1–12.
42 A. Y. Zhu, W. T. Chen, A. Zaidi, Y. W. Huang, M. Khorasaninejad, V. Sanjeev, C. W. Qiu and F. Capasso, *Light: Sci. Appl.*, 2018, **7**, 17158.
43 A. Ahmadivand, M. Semmlinger, L. Dong, B. Gerislioglu, P. Nordlander and N. J. Halas, *Nano Lett.*, 2019, **19**, 605–611.
44 K. Huang, J. Deng, H. S. Leong, S. L. K. Yap, R. Bin Yang, J. Teng and H. Liu, *Laser Photonics Rev.*, 2019, **13**, 1–9.
45 T. Kaelberer, V. A. Fedotov, N. Papasimakis, D. P. Tsai and N. I. Zheludev, *Science*, 2010, **330**, 1510–1512.
46 A. Ahmadivand, B. Gerislioglu, R. Ahuja and Y. Kumar Mishra, *Mater. Today*, 2020, **32**, 108–130.
47 P. Zheng, Q. Dai, Z. Li, Z. Ye, J. Xiong, H. C. Liu, G. Zheng and S. Zhang, *Sci. Adv.*, 2021, **7**, 363–384.